Theoretical study of structure sensitivity on ceria-supported single platinum atoms and its influence on carbon monoxide adsorption

Antoine Salichon, Agustin Salcedo, Carine Michel, David Loffreda

▶ **To cite this version:**

Antoine Salichon, Agustin Salcedo, Carine Michel, David Loffreda. Theoretical study of structure sensitivity on ceria-supported single platinum atoms and its influence on carbon monoxide adsorption. Journal of Computational Chemistry, 2024, 45 (25), pp.2167-2179. 10.1002/jcc.27393 . hal-04728557

HAL Id: hal-04728557
https://hal.science/hal-04728557v1

Submitted on 21 Oct 2024

HAL is a multi-disciplinary open access archive for the deposit and dissemination of scientific research documents, whether they are published or not. The documents may come from teaching and research institutions in France or abroad, or from public or private research centers.

L'archive ouverte pluridisciplinaire **HAL**, est destinée au dépôt et à la diffusion de documents scientifiques de niveau recherche, publiés ou non, émanant des établissements d'enseignement et de recherche français ou étrangers, des laboratoires publics ou privés.

Theoretical Study of Structure Sensitivity on Ceria-Supported Single Platinum Atoms and its Influence on Carbon Monoxide Adsorption

Antoine Salichon, Agustin Salcedo, Carine Michel and David Loffreda*

ENSL, CNRS, Laboratoire de Chimie UMR 5182, 46 Allée d'Italie, 69364 Lyon Cedex, France

*Correspondence to David Loffreda (E-mail: *david.loffreda@ens-lyon.fr*)

ABSTRACT

Density functional theory (DFT) calculations explore the stability of a single platinum atom on various flat, stepped and defective ceria surfaces, in the context of Single-Atom Catalysts (SAC) for the Water-Gas Shift (WGS) reaction. The adsorption properties and diffusion kinetics of the metal strongly depend on the support termination with large stability on metastable and stepped CeO_2(100) and (210) surfaces where the diffusion of the platinum atom is hindered. At the opposite, the more stable CeO_2(111) and (110) terminations weakly bind the platinum atom and can promote the growth of metallic clusters thanks to fast diffusion kinetics. The adsorption of carbon monoxide on the single platinum atom supported on the various ceria terminations is also sensitive to the surface structure. Carbon monoxide weakly binds to the single platinum atom supported on reduced CeO_2(111) and (211) terminations. The desorption of the CO_2 formed during the WGS reaction is thus facilitated on the latter terminations. A vibrational analysis underlines the significant changes in the calculated scaled anharmonic CO stretching frequency on these catalysts.

Keywords: Density Functional Theory, Single-Atom Catalysis, Structure Sensitivity, Platinum, Ceria, Carbon Monoxide, Water-Gas Shift Reaction

1. Introduction

The pressing issue of global warming raises the real challenge of producing clean energy, in particular for the automotive industry and the production of pure hydrogen for proton exchange membrane fuel cells (PEMFC).[1] Currently, the steam reforming of methane ($CH_4 + H_2O \rightarrow CO + 3H_2$) catalyzed by nickel-based catalysts is the most widespread hydrogen synthesis method at the industrial level. This reaction generates carbon monoxide as a by-product which is then eliminated via the exothermic Water-Gas Shift (WGS) reaction, also producing hydrogen ($CO + H_2O \rightarrow CO_2 + H_2$).

To optimize this process and produce pure hydrogen in greater quantities, it is necessary to develop new catalysts. The catalyst historically used for WGS ($Cu/ZnO/Al_2O_3$) has many drawbacks.[1,2] For instance, it has to operate continuously, not exceed 330 °C to avoid copper sintering and it is easily poisoned by oxygen and sulfur compounds such as dimethyl sulphide.[1,3,4] This is why catalysts based on noble metals such as platinum,[5] stable at high temperatures and resistant to poisons, are the most studied materials for WGS.[6] These noble metal-based catalysts have nonetheless a high cost, which prevents their massive deployment at the industrial scale. Among the noble metals, platinum belongs to the most active materials for CO oxidation and WGS.[7,8,9] Low amounts of the metal may be enough for achieving a good catalytic performance. The choice of the support is also of primary importance for WGS. Indeed,

platinum-based catalysts on reducible supports such as ceria and titania are up to thirty times more active than on irreducible supports such as alumina.[7]

Concerning the reactivity, one hypothesis supports a bifunctional mechanism where platinum preferentially adsorbs CO and its oxidation into CO_2 rather occurs at the interface with the reducible support. The generated oxygen vacancy promotes water dissociation, thus explaining the importance of considering reducible supports.[7] Among them, ceria has been widely studied for many years because of its high oxygen transport and storage capacity associated with the change of oxidation states between Ce^{4+} and Ce^{3+}.[10,11] A strong electronic transfer from Pt to ceria is expected. An excess of oxygen especially at the Pt/CeO_2 interface promotes the oxidation of carbon monoxide resulting in an activity increase for the metal.[1,10,12] Pt/CeO_2 thus appears as a very interesting catalyst for WGS.[13]

The size of the metal particles is also of great importance. For Pt/CeO_2 catalysts, nanoclusters, with a diameter of 3.8 nm and supported on ceria, exhibit a large turnover frequency (TOF)[11] while outperforming single-atom catalysts (SAC). At a smaller size of 1.4 nm, other authors have found a higher activity for reduced nanoparticles compared to highly dispersed Pt^{2+} species.[14] Another key parameter is the change in the initial morphology of the catalyst, due to temperature or to gaseous atmosphere variations especially during the reaction. New active sites for WGS can indeed be created by reconstruction of metallic nanostructures.[15] The control of the dispersion of platinum on ceria also represents a major challenge in the development of more efficient catalysts. For instance, redispersion in the presence of oxygen takes place from 400°C and allows the formation of SAC, namely Pt_1/CeO_2.[14]

Pt/CeO_2 SACs have several drawbacks currently preventing them from being used industrially. First, during the adsorption of CO, the Pt-C bond is very strong.[15] The desorption of the products is thus complicated, and the catalytic activity of these materials is consequently low. Another challenge is the control of sintering leading to metallic nanoclusters, due to the high surface energy of this type of catalyst.[15] To limit sintering, small amounts of platinum are used during the synthesis, but the corresponding catalytic performance is lower than those of nanoclusters.[15] However, new treatment methods tend to limit sintering and stabilize Pt_1/CeO_2 catalysts. A steam treatment at T=750 °C can create surface oxygen vacancies responsible for ceria activation without a reducing agent, promoting the formation of hydroxyl groups in presence of water.[16,17] The isolated Pt atoms at the vicinity of these OH species are then kinetically stable at temperatures above 800°C and the oxidation of CO is greatly improved at low temperatures.[16,17] Nie *et al.* have compared such treatment with conventional high temperature ageing in air, by showing that an oxidizing treatment only generates strong Pt-O-Ce bonds which inhibit CO oxidation.[17] Hence such a pre-treated Pt_1/CeO_2 catalyst is active at 60°C and it reaches a conversion of 100% from 148°C, whereas a conventional Pt_1/CeO_2 catalyst only shows a significant performance at higher temperature (210°C).[17] Overall the study of the surface sensitivity of an isolated platinum atom on different ceria surfaces could lead to a compromise between the strength of the Pt-O-Ce bond and the dispersion of platinum.

Experimentally, the catalyst active phase agglomerates on the most thermodynamically stable termination $CeO_2(111)$.[2] Wu *et al.* have highlighted the importance of the nature of the surface for nanoparticle catalysts. Indeed, the redispersion of platinum after various oxidizing and reducing treatments at 600°C takes place only on stepped $CeO_2(100)$ but not on flatter $CeO_2(111)$.[18] Despite significant experimental efforts investigating the performance of Pt-

based SAC for WGS, there is a lack of *operando* measurements and characterization explaining the structure sensitivity.

At the theoretical level, clean ceria surfaces have been extensively studied in the literature over the past twenty years. DFT and DFT+U calculations at the GGA level have shown that the CeO_2(111) termination is thermodynamically the most stable surface in vacuum at 0 K, but also at a high temperature of 300°C and partial oxygen pressures up to 1 atm.[19,20] The second most stable termination is CeO_2(110). The modified CeO_2(100) termination, where half of the surface oxygen atoms are removed, presents also a low surface energy, although less competitive than the two previous surfaces.[20,21,22,23] (211) and (210) stepped ceria surfaces could be competitive as well, but very few computational efforts have been conceded to date.[23] Several DFT studies have reported on the structure and the stability of atomically dispersed Pt on both low-index and high-index stepped ceria surfaces.[24,25,26,27,28,29,30] Other authors have investigated the interaction of Pt clusters on this support. [31,32,33,34,35] Smaller systems such as Pt dimers on CeO_2(111) have been modeled at the DFT+U level. Bruix *et al.* have shown that dimers form easily but they eventually agglomerate into larger clusters, confirming experimental results.[36] Regarding theoretical models of SACs, the study of the adsorption of isolated platinum atoms on CeO_2(111) has shown that the formation of metallic clusters on this surface was favorable.[37] The agglomeration of isolated platinum atoms would be more difficult on CeO_2(110) and platinum would be here in Pt^{2+} form.[37,38] The interaction between the platinum and the support is expected to be even stronger with the (100) surface.[37,30] Concerning the WGS reaction mechanism, a few DFT studies have investigated the elementary steps, showing the key role of oxygen vacancies and carboxylate species.[39,40,41,42,43] CO oxidation has also been investigated by DFT calculations on single platinum atom catalysts on (111), (100) and (110) surfaces.[44,45,46] The authors have found that it follows the Mars–van Krevelen mechanism where the single platinum atom acts as the electron acceptor/donor in the redox processes during the whole catalytic cycle.[44] Several gaps remain in the state-of-the-art of DFT models of Pt_1/CeO_2 catalysts. First, only few studies have considered the role of van der Waals interactions and spin-polarization, two properties which can have a non-negligible impact on the total electronic energy, on the optimized structures and on consequent analyses. In addition, the modeled ceria surfaces for the adsorption of platinum are mostly the (111) and (110) terminations, whereas very few studies have highlighted the stability of isolated atoms on the experimentally observed (100) and stepped (211) and (210) surfaces. Furthermore, a systematic study of potential energy surfaces predicting the most favorable adsorption structures of a single platinum atom and diffusion kinetics on all the competitive ceria terminations is missing in the literature to date. Similarly, a study on the nucleation and growth of platinum clusters of a few atoms based on diffusion kinetics has never been reported so far.

In this work, the structure sensitivity of the adsorption of an isolated platinum atom on different competitive ceria surfaces is explored by DFT+U calculations including spin polarization and van der Waals interactions. A systematic comparison of potential energy surfaces capturing adsorption thermodynamics and diffusion kinetics of Pt_1/CeO_2(hkl) is exposed. Then the adsorption of CO on the most stable Pt_1/CeO_2(hkl) catalysts is modeled and analyzed through thermodynamics and molecular vibrations.

2. Computational Methods

Spin-polarized DFT calculations based on the Generalized Gradient Approximation (GGA) have been performed using the VASP code (version 6.2.0).[47,48,49,50] The Perdew-Burke-Ernzerhof (PBE) functional[51] has been chosen and the long-range van der Waals interactions have been described by the semi-empirical DFT-D3 Becke-

Johnson correction method (noted D3(BJ)).[52,53] The DFT+U approach has been implemented with Dudarev's scheme[54] to consider the localization of Ce 4f valence electrons, as suggested previously by other studies.[55,56,57,58,59] The semi-empirical Hubbard term U_{eff} has been set to 4.5 eV.[60,61] The interactions between electrons and ion cores have been described by potentials generated by the Projector Augmented-Wave method.[62] Valence electrons have been described with plane wave basis sets with a cut-off energy of 400 eV. For surface models, a large vacuum space of 15 Å has been considered to separate equivalent periodic slabs along the z axis. Concerning the dispersion in the Brillouin zone, a Monkhorst-Pack k-points grid of (13x13x13) has been chosen for the CeO_2 bulk. For the surface models, k-point grids of (9x11x1), (13x9x1), (13x13x1), (7x9x1) and (7x5x1) have been selected for the (111), (110), (100), (211) and (210) terminations, respectively. The clean ceria surface supercells are defined in Table 1 for non-symmetric slabs and in Table S1 of the Supplementary Material for symmetric slabs. The adsorption of platinum and carbon monoxide has been modeled only on one side of the slabs, thus leading to non-symmetrically relaxed ceria systems. After geometry optimization (complete relaxation of symmetric slabs and relaxation on one side for non-symmetric slabs), the stability of a given termination has been determined by evaluating its surface energy ($J.m^{-2}$) as follows:

$$\mathrm{E_{surf}} = (\mathrm{E}(CeO_2(\mathrm{hkl})) - \mathrm{E}(CeO_2(\mathrm{bulk})))/2 \times \mathrm{A} \quad (1)$$

In this formula, $E(CeO_2(hkl))$ corresponds to the total electronic energy of the surface model of (hkl) termination. The corresponding surface areas A are 51, 42, 29, 72 and 66 $Å^2$ for CeO_2(111), (110), (100), (211) and (210) terminations, respectively. For symmetric slabs (Table S1), the computed surface energies are exact since both surfaces are identically relaxed in each case. For non-symmetric slabs (Table 1), the reported surface energies correspond to average values of relaxed and unrelaxed surfaces. $E(CeO_2(bulk))$ is the total energy of the CeO_2 bulk. For stoichiometric surface models, the total electronic energy of the stoichiometric ceria bulk is considered. For non-stoichiometric surface models, the total electronic energy of an equivalent non-stoichiometric bulk CeO_{2-y} is calculated as follows:

$$\mathrm{E}(CeO_{2-y}(\mathrm{bulk})) = \mathrm{Nb_{Ce}} \times \mathrm{E_{Ce}} + \mathrm{Nb_O} \times \mathrm{E_O} + \mathrm{Nb_{Ce}} \times \mathrm{E_{Ce-O}} \times \mathrm{Nb_{bond/Ce}} \quad (2)$$

Nb_{Ce} and Nb_O correspond to the number of cerium and oxygen atoms of the considered model. E_{Ce} and E_O are the energies of the isolated cerium and oxygen atoms (-0.90 eV and -1.67 eV, respectively). Finally, E_{Ce-O} (-2.62 $eV.bond^{-1}$) corresponds to the Ce-O bonding energy in the stoichiometric CeO_2 bulk which is derived from the total cohesion energy of the ceria bulk normalized by its number of Ce-O chemical bonds.

In all the DFT+U calculations of Pt_1/CeO_2(hkl) models performed for the elaboration of potential energy surfaces (PES), spin polarization has not been considered, except for the reduced CeO_2(111) surface, due the presence of magnetic Ce^{3+} cations associated with the oxygen vacancy. Nonetheless, spin-polarized DFT+U calculations have then been performed systematically to refine the adsorption structures of Pt_1/CeO_2(hkl), of which the starting geometries have been extracted from the lowest potential energy wells on the maps (see Table S2 for all the considered magnetic states and their relative stability). For the pristine and lowly corrugated (111), (110) and (211) surfaces, the density of points considered on the PES for the adsorption of Pt are 8 points.$Å^{-2}$, 10 points.$Å^{-2}$ and 6 points.$Å^{-2}$, respectively. For the (100) and (210) stepped surfaces, the chosen point density is increased (15 points. $Å^{-2}$) due to the larger corrugation and structure complexity. The PES have been interpolated from the adsorption energies obtained after geometry optimizations of Pt_1 in interaction with CeO_2(hkl), at specific frozen

positions (x,y) on regular grids (relaxing all the other degrees of freedom of Pt_1, and of the surface atomic planes of CeO_2(hkl)). At each (x,y) point of the grid, the corresponding adsorption energy of the platinum atom ($E_{ads}(Pt_1/CeO_2(hkl)(x,y))$) has been defined as follows and this has helped to determine the most stable nucleation sites on CeO_2(hkl):

$$E_{ads}(Pt_1/CeO_2(hkl)(x,y)) = E(Pt_1/CeO_2(hkl)(x,y)) - (E(CeO_2(hkl)) + E(Pt)) \quad (3)$$

where $E(Pt_1/CeO_2(hkl)(x,y))$ corresponds to the total electronic energy of the Pt_1/CeO_2(hkl) relaxed system. $E(CeO_2(hkl))$ and E(Pt) are the total electronic energies of the considered clean surface and of the isolated platinum atom, respectively. This definition of adsorption energy is general and also valid for refined adsorption structures.

For all the refined geometry optimizations, tight convergence criteria have been considered for total electronic energy (10^{-6} eV) and residual forces on the nuclei (0.01 eV.Å^{-1}). These convergence criteria have been lighter for the elaboration of PES due to the expensive computational effort (10^{-4} eV and 0.05 eV.Å^{-1}, respectively). For all the geometry optimizations of Pt_1/CeO_2(hkl) non-symmetric slab models, and for CO adsorption, the bottom atomic layers of ceria have been kept frozen to the bulk optimal structure, whereas all the degrees of freedom of the surface atomic planes of ceria and those of Pt and CO have been completely relaxed. In the PES, the (x,y) coordinates of platinum have been kept frozen.

To compare the absolute stability between Pt_1/CeO_2(hkl) catalysts, the excess energy (J.m^{-2}) has been evaluated as follows:

$$E_{exc} = (E(Pt_1/CeO_2(hkl)) - E(Pt) - E(Bulk))/Area \quad (4)$$

with the same definitions for each component as in equations (1) and (3). The excess energy, which is positive in our study, contains two contributions opposite in sign: the adsorption energy of the single platinum atom on a given CeO_2(hkl) termination (stabilizing and minority component normalized here by the surface area) and the surface energy related to the cost of creating CeO_2(hkl) with respect to the ceria bulk (destabilizing majority component).

From the PES of Pt_1/CeO_2(hkl) catalysts, the most likely diffusion pathways of platinum on ceria can be predicted. Diffusion activation barriers can then be calculated along the x and y directions ($E_a(x)$ and $E_a(y)$, respectively). They correspond to the energy differences between the highest energy point along the considered direction and the global minimum.

After the investigation of the adsorption of a single platinum atom on all the considered ceria terminations (nucleation process), the elaboration of PES for the formation of Pt dimers and trimers has been performed only on the reduced CeO_{2-x}(111) termination (single oxygen vacancy) starting from the most stable Pt_1 (for dimer formation) and Pt_2 (for trimer formation) adsorption structures (growth processes). The corresponding PES have been exposed in the Supplementary Material (Figures S1 and S2). For Pt_2 adsorption on the CeO_{2-x}(111) surface model, three possible definitions of adsorption energy have been considered: first, the associative adsorption of a second platinum atom on the most stable Pt_1/CeO_{2-x}(111) relaxed structure (corresponding to position x=0.25 and y=0.50 in Figure 2b)):

$$E_{ads,associative}(Pt_2/CeO_{2-x}(111)(x,y)) = E(Pt_2/CeO_{2-x}(111)(x,y)) - (E(Pt_1/CeO_{2-x}(111)(x=0.25,y=0.50)) + E(Pt)) \quad (5)$$

Second, the adsorption of an isolated Pt_2 dimer on CeO_{2-x}(111):

$$E_{ads,dimer}(Pt_2/CeO_{2-x}(111)(x,y)) = E(Pt_2/CeO_{2-x}(111)(x,y)) - (E(CeO_{2-x}(111)) + E(Pt_2)) \quad (6)$$

Third, the coadsorption of two Pt atoms on CeO_{2-x}(111):

$$E_{coads}(Pt_2/CeO_{2-x}(111)(x,y)) = E(Pt_2/CeO_{2-x}(111)(x,y)) - (E(CeO_{2-x}(111)) + 2E(Pt)) \quad (7)$$

In Eq. (5)-(7), $E(Pt_2/CeO_{2-x}(111)(x,y))$ corresponds to the total electronic energy of the Pt_2/CeO_{2-x}(111) system when the second platinum atom is adsorbed at positions (x,y) on the corresponding supercell. $E(Pt_2)$ is the total electronic energy of the gas phase Pt_2 dimer. $E(CeO_{2-x}(111))$ corresponds to the total electronic energy of the clean CeO_{2-x}(111) reduced surface.

Following the same ideas, the adsorption of Pt_3 trimer on the reduced CeO_{2-x}(111) surface can be considered as a coadsorption of three Pt atoms on CeO_{2-x}(111) or the associative adsorption of one Pt atom on Pt_2/CeO_{2-x}(111):

$$E_{coads}(Pt_3/CeO_{2-x}(111)(x,y)) = E(Pt_3/CeO_{2-x}(111)(x,y)) - (E(CeO_{2-x}(111)) + 3E(Pt)) \quad (8)$$

$$E_{ads,associative}(Pt_3/CeO_{2-x}(111)(x,y)) = E(Pt_3/CeO_{2-x}(111)(x,y)) - (E(Pt_2/CeO_{2-x}(111)) + E(Pt)) \quad (9)$$

In Eq. (8)-(9), $E(Pt_3/CeO_{2-x}(111)(x,y))$ corresponds to the total electronic energy of the Pt_3/CeO_{2-x}(111) system when the third platinum atom is adsorbed at positions (x,y) on the optimal Pt_2/CeO_{2-x}(111) catalyst.

CO adsorption has then been considered on the most stable adsorption sites of Pt_1/CeO_2(hkl) catalysts. Spin polarization has been included in all the geometry optimizations at the DFT+U level, and various magnetic states have been optimized and compared systematically (see Table S3). The adsorption energy of the molecule has been computed as follows:

$$E_{ads}(CO@Pt_1/CeO_{2-y}(hkl)) = E(CO@Pt_1/CeO_{2-y}(hkl)) - (E(Pt_1/CeO_{2-y}(hkl)) + E(CO)) \quad (10)$$

where $E(CO@Pt_1/CeO_{2-y}(hkl))$ is the total electronic energy of CO adsorbed on the Pt_1/CeO_2(hkl) system, $E(Pt_1/CeO_{2-y}(hkl))$ being the total electronic energy of the most stable adsorption site and magnetic state of Pt_1 adsorbed on CeO_{2-y}(hkl), and E(CO) being the total electronic energy of CO gas phase.

The vibrational analysis of the optimal $CO@Pt_1/CeO_2$(hkl) systems has been carried out by using the finite difference approach on forces based on small variations of atomic positions around the optimized equilibrium geometries (harmonic approximation). The harmonic frequencies and corresponding normal modes have been evaluated by the diagonalization of the Hessian matrix obtained with atomic displacements of 0.02 Å. All the degrees of freedom of relaxed surface ceria, adsorbed Pt and CO have been included in the calculations. Vibrations have been calculated at the restricted level and the convergence parameters have been the same as those for the geometry optimizations. Anharmonic corrections to harmonic CO stretching frequencies have been determined by fitting the potential energy around the equilibrium state in the space of the normal mode coordinates with a third-order development of the Morse potential. In addition, all CO stretching frequencies have been scaled by a factor of 1.0227, chosen so that the calculated stretching frequency of gas-phase CO matches perfectly the experimental value (2143 cm^{-1}).

3. Results and discussion

3.1 Ceria surface models

CeO_2 bulk

To validate our methodology for describing ceria surfaces, the CeO_2 bulk was initially optimized. In the crystalline structure of this insulating rare earth oxide (cubic fluorite structure), eight oxygen atoms form a cube, and each one is bonded to four cerium atoms within a tetrahedron. A 13×13×13 grid of k-points allows for a numerical accuracy of 2.6×10^{-5} eV on total electronic energy (equivalent to 23×23×23 k-point grid). The calculated lattice parameter a_0 (5.42 Å) at the PBE-D3(BJ) level is very close to the experiment value (5.41 Å) and appears to be slightly more accurate than the one obtained at the standard GGA PBE level (5.38 Å).[21,63] Furthermore, the computed bulk modulus (187 GPa) is also in good agreement with experiments (174±17 GPa).[63] The bulk model is thus validated and serves as the starting point for the construction of the geometries of different ceria surface terminations.

Competitive ceria surfaces

Five ceria surface terminations were modeled: CeO_2(111), CeO_2(110), CeO_2(211), CeO_2(100) and CeO_2(210). According to Jiang *et al.*, those terminations present low surface energies after geometry optimizations at the GGA PBE level ($0.45 < E_{surf} < 1.21$ J.m^{-2}).[20] These surfaces have several possible terminations (Ce, O-top, O-hollow, CeO_2 and CeO, depending on the (hkl) surface orientation) which can lead to stoichiometric or non-stoichiometric, polar or non-polar systems. Pristine or modified slab models were considered. Among modifications, neutralized slab models were defined when non polar systems are created to represent intrinsically polar surfaces.[22] Hence the surface energies of all the possible terminations of each surface were calculated first to determine the most stable systems.

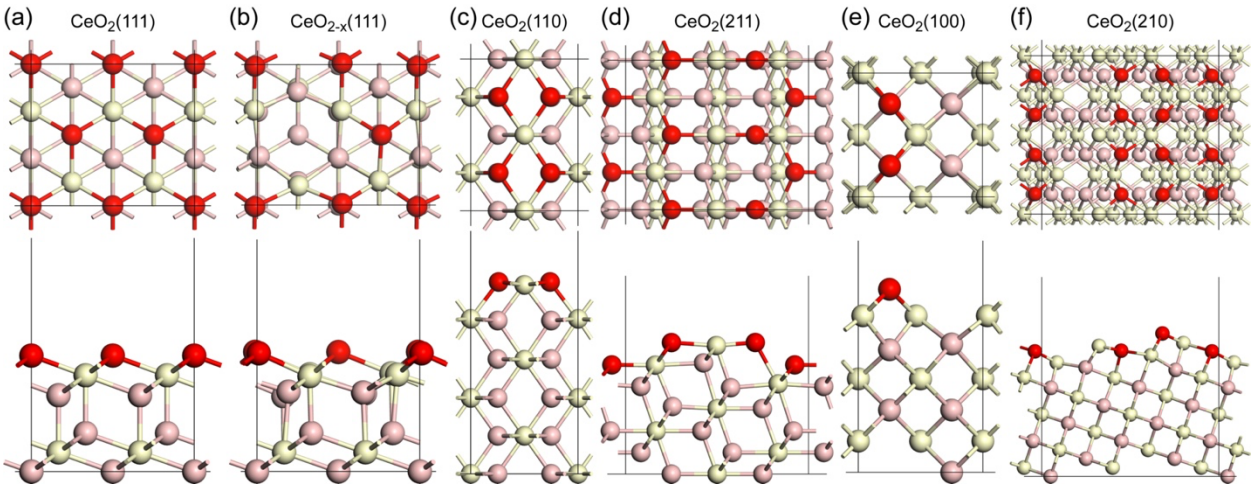

FIGURE 1 Lateral and top views of optimized non-symmetric slabs related to most stable clean ceria surfaces: (a) pristine, flat and stoichiometric (111) surface (6 atomic planes); (b), reduced non-stoichiometric (111) surface with a single surface oxygen vacancy (6 atomic planes); (c) pristine, flat and stoichiometric (110) surface (6 atomic planes); (d) pristine, flat and stoichiometric (211) surface (7 atomic planes); (e) neutralized, stepped and stoichiometric (100) surface (7 atomic planes); (f) neutralized, stepped and stoichiometric (210) surface (9 atomic planes). Ce and surface O atoms are depicted in light gray and red, respectively; O atoms belonging to underlying layers in light red.

The most stable terminations are depicted in Figure 1. All the retained surface models are stoichiometric; pristine and neutral for CeO_2(111), (110), (211). Due to the high polarity and intrinsic instability of the two latter CeO_2(100) and CeO_2(210) terminations, half of the oxygen atoms belonging to the outermost atomic planes have been removed to neutralize the surface models.[22] The most stable ceria surfaces exhibit different supercells, numbers of atomic planes, and k-points grids, as recalled in Table 1. The most stable termination of CeO_2(111) is O_{hollow}-terminated (Figure 1(a)), whereas CeO_2(110) (Figure 1(c)) and CeO_2(211) (Figure 1(d)) surfaces have a unique mixed CeO_2 termination. The neutralized CeO_2 (100) (Figure 1(e)) and (210) (Figure 1(f)) surfaces are characterized by their O_{step} and mixed Ce-O_{step} terminations, respectively. The relative stability order obtained by calculating surface energies is the following: (111) > (110) > (211) > (210) > (100) (see Table 1). The computed average Ce-O bonding energies show a compatible trend with this result. Hence CeO_2(111) is the thermodynamic termination for ceria with the lowest surface energy of 0.95 J.m^{-2}, in agreement with experiments, and the relative stability order is similar to previous studies.[20,33] A non-stoichiometric surface model of reduced CeO_{2-x}(111) has also been generated by considering the optimal structure of CeO_2(111) and by creating a single oxygen vacancy on the relaxed side of the slab (Figure 1(b)). The spin-polarized calculation of the clean reduced ceria surface has shown that the two electrons, released by the creation of the oxygen vacancy, are collected by two adjacent surface cerium atoms become Ce^{3+} at the vicinity of the vacancy, leading to a triplet state, which is found as the most stable magnetic state for the considered supercell. With a surface energy of 1.93 J.m^{-2}, the reduced surface model CeO_{2-x}(111) appears less stable than pristine CeO_2(111) and (110), but more stable than CeO_2(211), (210) and (100).

TABLE 1 Energetics of optimized clean most stable ceria surfaces (at the unrestricted PBE-D3(BJ)+U level). The non-symmetric slabs used to consider the adsorption properties have been reported here and correspond to the illustrations shown in Figure 1. The bottommost atomic planes are kept frozen to the ideal bulk structure, while the topmost atomic planes are relaxed, thus leading to two different surfaces (relaxed and unrelaxed). The different ceria surfaces are either pristine, reduced with the presence of a single oxygen vacancy, or neutralized by changing the composition of the terminal atomic planes by removing oxygen atoms. The surfaces are either stoichiometric or non-stoichiometric (reduced) and the compositions of terminations are reported. The number of atomic planes is addressed together with the chosen supercells and related k-points grids. The average surface energy (J.m^{-2}), total magnetization (μB) and average Ce-O bonding energy (eV/bond) are reported.

CeO_{2-y}(hkl)	CeO_2(111)	CeO_{2-x}(111)	CeO_2(110)	CeO_2(211)	CeO_2(100)	CeO_2(210)
	pristine stoichiometric flat	reduced non-stoichiometric flat	pristine stoichiometric flat	pristine stoichiometric stepped	neutralized stoichiometric stepped	neutralized stoichiometric stepped
Termination	O_{hollow}	O_{hollow}	Mixed CeO_2	Mixed CeO_2	O_{step}	Mixed Ce-O_{step}
Supercell	$p(\sqrt{2}\times\sqrt{6})R90°$	$p(\sqrt{2}\times\sqrt{6})R90°$	$p(1\times\sqrt{2})R90°$	$p(\sqrt{3}\times\sqrt{2})R90°$	$p(1\times1)R90°$	$p(2\times\sqrt{5})R90°$
Number of atomic planes	6	6	6	7	7	9
k-points grid	9×11×1	9×11×1	13×9×1	7×9×1	13×13×1	7×5×1
Average surface energy (J.m^{-2})	0.95	1.93	1.46	2.01	2.61	2.44
M (μB)	0	2	0	0	0	0
Ce-O bonding energy (eV/bond)	-2.53	-2.43	-2.54	-2.46	-2.42	-2.47

3.2 Adsorption of Pt_1 on ceria surfaces

Pt_1 adsorption on pristine CeO_2(111), CeO_2(110) and CeO_2(211) surfaces

In the case of the adsorption of a single platinum atom on the stoichiometric and pristine CeO_2(111) surface model, the most stable position according to the PES is a bridge structure between two surface oxygen atoms (see all the equivalent lowest potential energy wells by symmetry on the PES in Figure 2(a) and the corresponding optimal structure in Figure 3(a)), in agreement with previous

studies.[24,27,28,29,30] The adsorption energy of the fully relaxed structure is quite exothermic (-2.97 eV as reported in Table 2, corresponding to triplet for the most stable magnetic state, as shown in Table S2 of the Supplementary Material). According to the potential energy map, the least favorable Pt position is on top of surface cerium atoms. We note that the maximum energy difference between all the adsorption points of the PES is not very large (about 1.3 eV) and that there are many equivalent local minima on this surface (see Figure 2(a)). By considering diffusion pathways from the most stable position and along x and y axis, the predicted diffusion barriers are low (0.11 eV) and equivalent along both directions. This result suggests that a single Pt atom can diffuse quite easily on CeO_2(111) and thus the formation of small clusters will not be limited by diffusion kinetics.

For the adsorption of Pt_1 on CeO_2(110), the most stable position according to the PES (Figure 2(c)) is also a bridge-bonded structure between two surface oxygen atoms (Figure 3(c) for the optimal geometry). The potential energy map shows a globally stronger adsorption on CeO_2(110), close to the minima, compared to CeO_2(111), and at the same time, a much less favorable interaction close to the maxima (on top of surface cerium atoms). The fully relaxed best adsorption structure presents an adsorption energy of -3.66 eV (Table 2, corresponding to triplet). Regarding diffusion kinetics, activation barriers on CeO_2(110) are significantly different with a clear preference along the y axis (0.48 eV versus 1.12 eV along x axis). This suggests a unidirectional diffusion of single Pt atoms along the y direction and thus a high propensity to form Pt dimers along this axis.

In the case of single Pt adsorption on CeO_2(211), the PES (Figure 2(d)) shows that the best position is once again a bridge structure above two surface oxygen atoms with a largely exothermic adsorption energy of -6.08 eV (see Figure 3(d) for the optimized structure and Table 2 for energetics, the best magnetic state being triplet). The overall increase of the adsorption strength is accompanied by a concomitant increase in activation barriers with 4.03 and 2.33 eV along x and y axis, respectively. Those high barriers prevent surface diffusion making CeO_2(211) a good candidate for generating single atom catalysts.

Pt_1 adsorption on neutralized CeO_2(100) and CeO_2(210) surfaces

Regarding the exploration of the adsorption of single platinum atom on neutralized CeO_2(100), the PES indicates that the best position (Figure 2(e)) is a bridge-bonded structure with two surface oxygen atoms[37] (Figure 3(e) for the optimal geometry). The higher metastability of this termination makes the adsorption process globally more exothermic in the whole energetic spectrum and even in the proximity of cerium surface atoms. The refined and fully relaxed structure of the most stable adsorption position presents a very strong adsorption energy of -6.04 eV and corresponds to singlet (Table 2). Concerning diffusion pathways, the PES clearly suggests large activation barriers along x (2.12 eV) and y axis (2.53 eV) starting from the most stable adsorption sites. Very strong adsorption and high diffusion barriers indicate a clear propensity to generate single atom catalysts on CeO_2(100).

In the case of the other neutralized termination CeO_2(210), the PES exposed in Figure 2(f) confirms once again that the adsorption of a single platinum atom on stepped ceria surfaces is very strong. The presence of defects leading to a significant metastability of this ceria termination promotes its interaction with platinum. The best position is a fourfold hollow on top of four surface oxygen atoms (Figure 3(f) for the optimized structure). The adsorption energy is the largest one (-7.93 eV) registered in this work (Table 2). Simultaneously, diffusion pathways of platinum on CeO_2(210) are completely hindered with very high activation barriers along x (2.91 eV) and y axis (3.29 eV). Hence the stepped neutralized CeO_2(210)

system appears as the best candidate to form single atom catalysts.

Pt_1 adsorption on reduced CeO_{2-x}(111) surface

The last considered system is the adsorption of a platinum atom on a reduced CeO_{2-x}(111), surface exhibiting a single surface oxygen vacancy (Figure 2(b) for the PES). The potential energy map (derived from spin polarized calculations) clearly demonstrates that the best position for adsorbing platinum is a top site vertically above the oxygen vacancy. In the optimized structure, platinum is bonded to three surface cerium atoms (see Figure 3(b)), the adsorption energy is quite large (-4.23 eV, Table 2) in agreement with previous works[28] and the corresponding magnetic state is singlet (no spin). The potential energy surface is quite steep and isoenergetic around the most favorable position, except where the platinum atom is on top of cerium surface atoms (maximum of energy). Regarding diffusion kinetics, the activation barriers are high (1.76 eV and 1.54 eV along the x and y directions, respectively), indicating that diffusion is not easy around oxygen vacancies. Those defects could thus trap single platinum atoms quite efficiently.

Comparison of Pt_1/CeO_{2-y}(hkl) systems: relative and absolute stability and diffusion properties

In the previous sections, the relative stability of platinum adsorption on the various ceria terminations was determined based on adsorption strength. Although interesting, this property cannot capture the absolute stability of nucleation sites when all the considered ceria terminations are present in the catalytic system. The excess energy reported in Table 2 is a relevant stability descriptor which combines both the adsorption strength of the platinum atom and the energetic cost to create the nucleation site with respect to a common reference (ceria bulk). The order in excess energy is the following: CeO_2(111) > CeO_2(110) > CeO_2(100) > CeO_2(211) > CeO_{2-x}(111) > CeO_2(210). Note that the adsorption energies of fully optimized structures of Pt_1/CeO_2(hkl) (Table 2) are close to the corresponding estimations from the interpolation on the PES (Figure 2), except for CeO_2(210) where the spin polarization has a strong stabilizing effect on the fully relaxed system. In addition, the fully optimized geometries of Pt_1/CeO_2(hkl) are also very similar to those obtained in the PES, except for the stepped CeO_2(211), where the position of one surface oxygen atom bound to platinum significantly relaxes. Such a global agreement validates our approach for elaborating potential energy maps. The energetic order in adsorption energy is the following: CeO_2(210) > CeO_2(211) > CeO_2(100) > CeO_{2-x}(111) > CeO_2(110) > CeO_2(111). Although the order is not the exact opposite to that of the excess energy, the stability of the ceria termination seems to play a key role in the overall adsorption process. This result is compatible with previous conclusions on (111), (100) and (111) surfaces.[37]

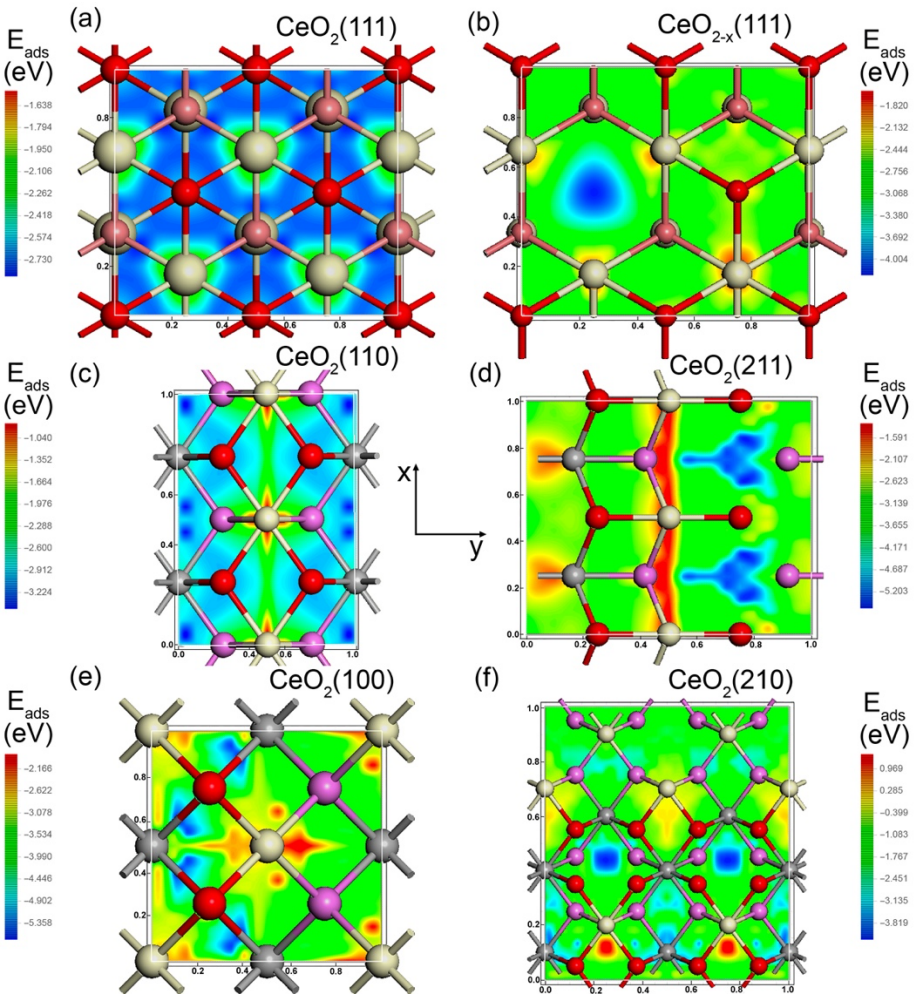

FIGURE 2 2D Potential energy maps on regular grids (x,y) (direct coordinates) for single Pt adsorption on various ceria surfaces (energetics being computed at the restricted PBE+U level, except for the reduced surface in (b) where PBE+U calculations were performed at the unrestricted level): (a) pristine flat (111); (b) reduced flat (111); (c) pristine flat (110); (d) pristine stepped (211); (e) pristine stepped (100); (f) pristine stepped (210) surfaces. The adsorption energy (eV) in the maps varies for the chosen ceria surface according to the reported color labeling in the vertical bars, defining the energetic spectrum in each case. Top views of the topmost ceria layers are drawn and superposed over the 2D energy maps to define in each case the correspondence between a specific energy point on the map and its geometric position on the ceria surface. Surface cerium and oxygen atoms are depicted in beige and red, respectively. Subsurface cerium and oxygen atoms are represented in grey and in light red or purple, respectively.

TABLE 2 Optimized adsorption structures of a single Pt atom (see Figure 3 for geometries) on the various ceria surfaces, at the unrestricted PBE+U level (most stable positions according to Figure 2). In each case, the adsorption site is mentioned together with the adsorption energy (eV) referred to the isolated Pt atom and the clean ceria surface, the excess energy ($J.m^{-2}$) referred to the ceria bulk, the total magnetization (μB), the optimal Pt-O distance (Å), and the diffusion activation barriers along the x and y directions predicted from the potential energy maps of Figure 2.

Pt_1/CeO_{2-y}(hkl)	CeO_2(111)	CeO_{2-x}(111)	CeO_2(110)	CeO_2(211)	CeO_2(100)	CeO_2(210)
Adsorption site	Bridge O_2	3-fold-hollow Ce_3	Bridge O_2	Bridge O_2	Bridge O_2	4-fold-hollow O
E_{ads} (eV)	-2.97	-4.23	-3.66	-6.08	-6.04	-7.93
E_{exc} ($J.m^{-2}$)	0.96	3.06	1.52	2.66	1.93	3.91
M (μB)	2	0	2	2	0	1.6
d(Pt-O) (Å)	2.15	-	2.08	2.00	2.01	1.97-2.00
d(Pt-Ce) (Å)	-	2.96	-	-	-	-
$E_{act,diff}$(x axis) (eV)	0.11	1.76	1.12	4.03	2.12	2.91
$E_{act,diff}$(y axis) (eV)	0.11	1.54	0.48	2.33	2.53	3.29

Regarding diffusion kinetics, the single platinum atom will easily move on the thermodynamically most stable CeO_2(111) surface and on the competitive CeO_2(110) termination, where activation barriers are remarkably low. On the other hand, diffusion will be quite impossible on the stepped CeO_2(210), CeO_2(211) and CeO_2(100) terminations where adsorption is really strong and activations barriers too high. Therefore, at a low content of deposited Pt, one can expect a larger propensity to form small clusters on CeO_2(111) and CeO_2(110) surfaces, but also a significant ability to further diffuse during the growth process, thus making the control of nanoparticle size and shape quite difficult. In contrast, on CeO_2(210), CeO_2(211) and CeO_2(100) surfaces, single-atom catalysts can be expected, however the strong adsorption on these defective terminations opens questions regarding the catalytic performance for the WGS reaction, especially for releasing the CO_2 product. The reduced CeO_{2-x}(111) surface model presenting a single oxygen vacancy appears as a good compromise for forming platinum clusters of a few atoms, with a sufficiently strong adsorption of the platinum atom, ensuring the control of isolated nucleation sites, and a concomitant moderately activated diffusion. Moreover, as mentioned in the Introduction, the ceria support undergoes reducing treatments which cause the generation of oxygen vacancies. This justifies our choice to investigate in the next step the formation of Pt_2 and Pt_3 multimers only on the reduced CeO_{2-x}(111) surface model.

3.3 Growth of platinum dimers and trimers on reduced CeO_{2-x}(111)

A potential energy surface has been elaborated for the interaction of two platinum atoms with the reduced ceria termination, by following the previous idea for single atom adsorption. The objective is the determination of the most likely adsorption structures for Pt_2 dimer on reduced CeO_{2-x}(111), as well as diffusion kinetics related to the dimer generation. To evaluate the stability of a second Pt atom (noted $Pt_{(2)}$) on the pre-covered CeO_{2-x}(111) surface by a first adsorbed Pt atom (noted $Pt_{(1)}$), a regular grid of frozen ($x\_Pt_{(2)}$,$y\_Pt_{(2)}$) positions has been considered on the most stable adsorbed structure for $Pt_{(1)}$, (see Figure 2(b) and Figure 3(b), where initially $x\_Pt_{(1)}$=0.25 and $y\_Pt_{(1)}$ =0.50).

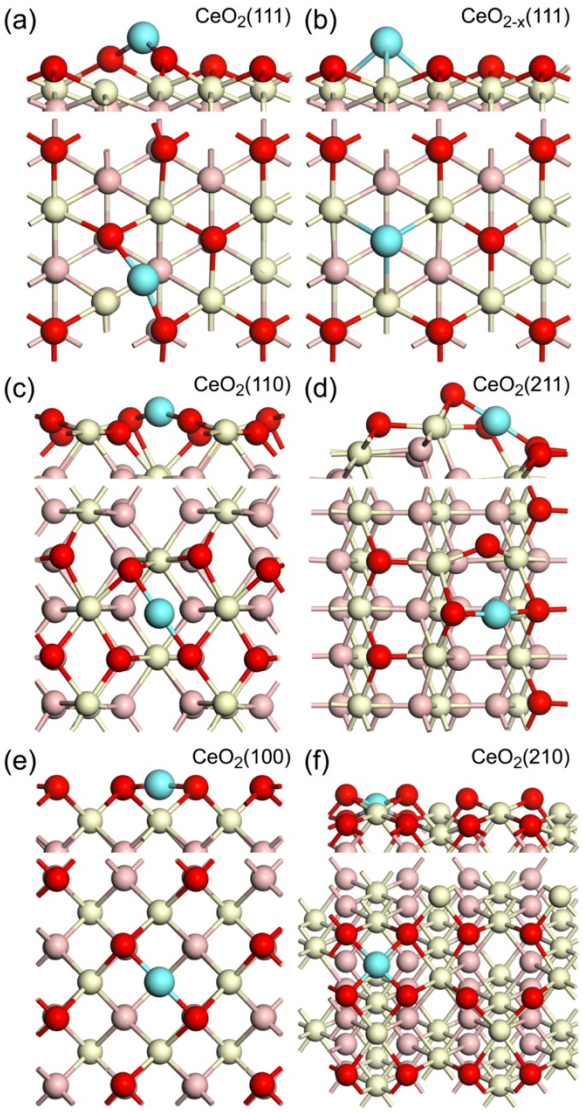

FIGURE 3 Lateral and top views of the optimized and most stable structures of a single Pt atom adsorbed on various ceria surfaces: (a) CeO_2(111), (b) reduced CeO_{2-x}(111), (c) CeO_2(110), (d) CeO_2(211), (e) CeO_2(100) and (f) CeO_2(210) (see Table 2 for other details and Figure 2 for potential energy maps). Cerium atoms are depicted in light gray, surface oxygen in red, subsurface oxygen in light red and platinum in light blue.

During the geometry optimizations, the degrees of freedom of $Pt_{(1)}$, of surface ceria atomic planes and of the z coordinate of $Pt_{(2)}$ are all allowed to

relax. The point density on the (x,y) grid is identical to that of $Pt_1/CeO_{2-x}(111)$. On the resulting PES reported in the Supplementary Material in Figure S1, six equivalent most stable positions of $Pt_{(2)}$ around $Pt_{(1)}$ located in the vacancy are seen. For the completely optimized structure (see Figure S2), on the one hand, the computed associative adsorption energy of $Pt_{(2)}$ on $Pt_{(1)}/CeO_{2-x}(111)$ is less exothermic (-3.85 eV, corresponding to an adsorption energy of the Pt_2 dimer of -4.45 eV) than the previously predicted stability of $Pt_{(1)}$ on the reduced surface (-4.23 eV). On the other hand, this energy is more exothermic than the one for the adsorption of $Pt_{(1)}$ on $CeO_2(111)$. This latter result can be explained by the energy gained upon formation of the Pt-Pt bond. It can also be seen in the value of the excess energy for adsorbed Pt_2 (1.85 $J.m^{-2}$), which is significantly lower than the one for $Pt_{(1)}/CeO_{2-x}(111)$ (3.06 $J.m^{-2}$). Regarding the optimal geometry, the platinum dimer adsorbs quasi-parallel to the ceria surface by binding to three surface cerium atoms and one surface oxygen (see Figure S2) and a significant elongation of the Pt-Pt bond (2.53 Å) is registered with respect to gas phase $Pt_2(g)$ (2.32 Å). No magnetism has been found. Note in passing that when the two Pt atoms are very close, they rearrange so that one of the two atoms is located on top of the other one in a bent or vertical configuration above the ceria support. Such a conformation is not competitive in stability as shown by the PES around $Pt_{(1)}$.

The determination of the most stable position of $Pt_{(2)}$ on the PES related to the platinum dimer on the reduced and pre-covered $Pt_{(1)}/CeO_{2-x}(111)$ surface (($x\_Pt_{(2)} = 0.40$, $y\_Pt_{(2)} = 0.80$) and ($x\_Pt_{(1)} = 0.25$ and $y\_Pt_{(1)} = 0.50$)) has served as a starting structure for the elaboration of another PES, aiming to predict the stability of a third platinum atom (noted $Pt_{(3)}$) on the dimer pre-covered $Pt_2/CeO_{2-x}(111)$ catalyst. As in the previous case, during the geometry optimizations, only the ($x\_Pt_{(3)}$, $y\_Pt_{(3)}$) coordinates of $Pt_{(3)}$ have been frozen at the points of a regular grid, while relaxing the degrees of freedom of the other atoms. The corresponding PES reported in Figure S3 of the Supplementary Material, suggests that $Pt_{(3)}$ prefers to bind to $Pt_{(1)}$ located on the oxygen vacancy to form a flat adsorbed trimer in a bent configuration (see Figure S4 for the optimized structure). The predicted associative adsorption energy (-5.03 eV) is even larger than those of $Pt_{(2)}$ and $Pt_{(1)}$ discussed previously. This suggests simultaneous stabilizing effects due to the formation of a second Pt-Pt bond and to the better interaction between the Pt_3 trimer and ceria support. Such a conclusion is reflected in the calculated excess energy (0.27 $J.m^{-2}$) which is by far more stable than the optimal $Pt_1/CeO_{2-x}(111)$ (3.06 $J.m^{-2}$) and $Pt_2/CeO_{2-x}(111)$ (1.85 $J.m^{-2}$) systems, but also more stable than $Pt_1/CeO_2(111)$ (0.96 $J.m^{-2}$). Hence, the cost of the oxygen vacancy formation is largely compensated by the formation of a Pt trimer and its interaction with such a defect. Moreover, according to the PES of Pt_1, Pt_2 and Pt_3 on $CeO_{2-x}(111)$, the diffusion activation barrier along y direction of one platinum atom is the highest one in the case of the trimer ($E_{act,diff}(y) = 1.80$ eV)) and the lowest one in the case of the dimer ($E_{act,diff}(y) = 1.09$ eV). For $Pt_1/CeO_{2-x}(111)$, the barrier is intermediate (1.45 eV). This shows that diffusion kinetics of small Pt clusters are strongly dependent on their size and the presence of an oxygen vacancy will tend to favor the formation of dimers.

Charge transfers based on the Bader analysis have also been computed for single platinum atom, dimer and trimer supported on the reduced $CeO_2(111)$ surface and presented in the Supplementary Material in Table S4. The charge transfer is opposite to the usual one for single platinum atom on pristine $CeO_2(111)$ surface, going from the defective ceria support to the platinum atoms which become negatively charged. Its amplitude progressively decreases with the increased size of the cluster, from 0.86 to 0.74 electron. The non-equivalence of the charge transfer between platinum atoms belonging to a given cluster is reflected by the asymmetry of the adsorption structure on the ceria support.

3.4 Adsorption and vibrations of CO on Pt_1/CeO_{2-y}(hkl)

After having explored the structure sensitivity of single platinum catalysts on ceria and how the selected reduced (111) termination impacts on the growth of small clusters, the adsorption properties of carbon monoxide are investigated in this section on various SACs. Indeed, CO is one of the reactants in the WGS reaction, for which the determination of the influence of the structure sensitivity on adsorption thermodynamics is particularly interesting. The typical onefold top (on Pt) and twofold bridge (between Pt and an adjacent O atom) adsorption structures for CO have been considered on the optimal Pt_1/CeO_{2-y}(hkl) catalysts and completely optimized, except for the reduced surface model, where the bridge position cannot be built due to the absence of a neighboring surface O atom to Pt. All the corresponding results are given in Table 3 and Figure 4, for the most stable and optimized structures. There are two families of SACs: strongly bound and moderately bound. In the cases of Pt_1/CeO_2(111), Pt_1/CeO_2(110) and Pt_1/CeO_2(211), CO adsorption is really strong (from -3.10 to -3.46 eV) and it causes a change in the active site, since the Pt atom moves from a bridge-bonded structure with surface oxygen atoms to a top position, as depicted in Figure 4. The best CO adsorption form is top and linear on the platinum atom, in agreement with Koleva *et al.*'s previous works,[64] reporting a stabilization of the Pt 5d orbitals due to a depopulation of the 5d projected states close to the Fermi level, when the metal is completely covered by CO. The best magnetic state can be either singlet or triplet. On the SACs related to stepped (100), (210) and reduced (111) surfaces, CO adsorption is more moderate (from -0.94 to -2.20 eV) and the Pt atom stays close to its optimal position, during CO adsorption. CO binds either linearly on top (CeO_{2-x}(111)) or through a CO_2 surface species (CeO_2(100) or CeO_2(210)). The best magnetic state is triplet on all these ceria terminations.

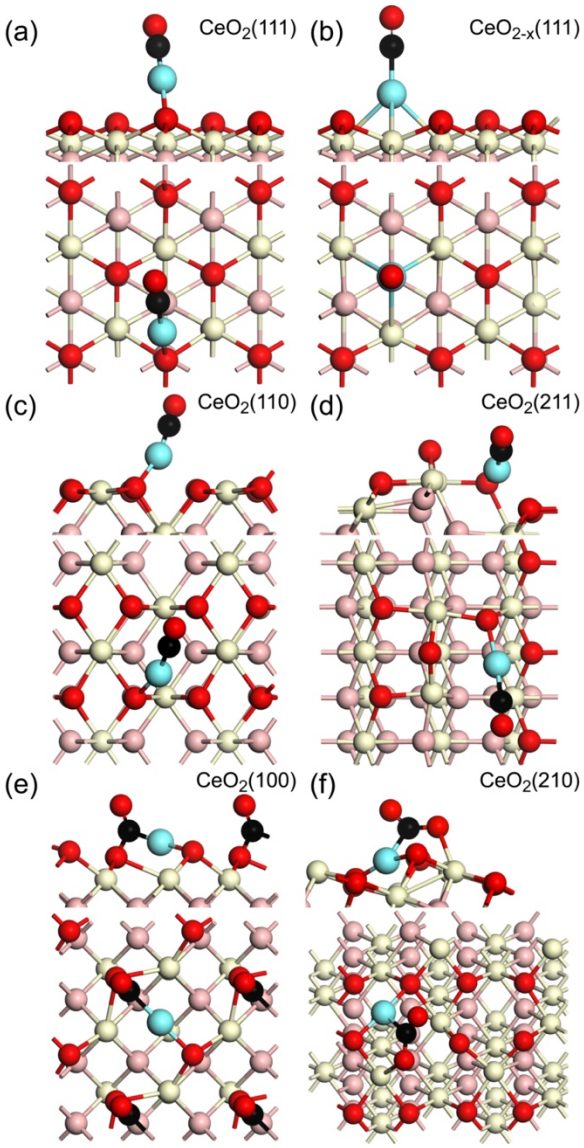

FIGURE 4 Lateral and top views of the optimized adsorption structures of CO on the SACs Pt_1/CeO_{2-y}(hkl): (a) CeO_2(111), (b) reduced CeO_{2-x}(111), (c) CeO_2(110), (d) CeO_2(211), (e) CeO_2(100) and (f) CeO_2(210) (see Table 3 for details and Figure 3 for optimized clean Pt_1/CeO_{2-y}(hkl) catalysts). Cerium atoms are depicted in light gray, oxygen belonging to the ceria surface and carbon monoxide in red, subsurface oxygen in light red, platinum in light blue and carbon in black. In (a-d), molecular adsorption of CO is registered on the ceria surfaces, while in (e-f), CO_2 adsorbed species form during CO chemisorption.

In the context of the WGS reaction, the activity of SACs is low due to the excessive strength of carbon monoxide adsorption and subsequent difficult desorption of the products. Our DFT models of SACs on thermodynamic terminations CeO_2(111), (110) and (211) support those

conclusions on the basis of CO adsorption thermodynamics. On the stepped (210) surface, the weakening of CO adsorption strength would be an interesting argument in favor of its catalytic activity for the WGS reaction, but this system is too high in absolute stability. The last two SACs on stepped CeO_2(100) and on the reduced CeO_{2-x}(111) exhibit the lowest adsorption energy for CO (with respective values of -1.95 and -0.94 eV), which make these SACs interesting for the WGS reaction. Nonetheless, on the (100) surface, the adsorption of CO in a CO_2 configuration might yield formate species in a H_2 environment compromising the desorption of CO_2 product. In this context, the Pt_1/CeO_{2-x}(111) catalytic system appears as our best candidate for WGS with concomitant moderate CO adsorption strength and sufficient absolute catalyst stability. Hence the key role of vacancies in the reaction mechanism evoked experimentally[41,42] finds here theoretical support.

The last part of this study deals with the vibrational analysis of CO on the SACs. A systematic harmonic vibrational analysis of the relaxed degrees of freedom of the optimized catalytic systems has been performed, underlining for instance a clear relationship between the CO adsorption energy and the Pt-CO stretching frequency as reported in Table 3 (the larger the adsorption strength the stronger the harmonic frequency). More interestingly, from the harmonic normal modes associated with the C-O stretching frequency (the one related to the CO molecule in the case of CO_2 surface species), scaled anharmonic values have been computed so that a direct comparison with experiments is possible. According to our predictions (Table 3), the relationship between adsorption energy, C-O equilibrium distance and scaled anharmonic C-O frequency is complex. The four top and linear adsorption forms present a scaled anharmonic value in the range 1982-2044 cm^{-1}. From infrared reflection absorption spectroscopy measurements of $Pt/CeO_2(111)/Cu(111)$ model catalysts,[65] CO first adsorbs on-top at step and edge sites on Pt nanoparticles (2066 cm^{-1}), before adsorbing on their (111) facets in bridging (1875 cm^{-1}) and on-top (2080-2097 cm^{-1}) positions. Those frequency ranges are compatible with other IR experiments.[66,67] On reduced CeO_{2-x}(111), a red-shifted band at 2053 cm^{-1} appears, which is attributed to an increased π-backbonding from Pt to CO, as a result of a change in electronic metal-oxide interaction.[65] In our work, a small red shift in frequency is also seen from Pt_1/CeO_2(111) (2044 cm^{-1}) to Pt_1/CeO_{2-x}(111) (2041 cm^{-1}) SACs, with a very good correspondence with measurements on Pt nanoparticles (from 2066 to 2053 cm^{-1}).

TABLE 3 Adsorption properties of CO adsorption on various Pt_1/CeO_{2-y}(hkl) catalysts, at the unrestricted PBE+U level (see Figure 4 for the optimized geometries). Adsorption site and state are reported with adsorption energy referred to gas phase CO molecule and clean catalyst (eV), total magnetization (μB), optimal Pt-C, Pt-O, Pt-Ce, C-O distances (Å), C-O stretching frequencies (at the scaled harmonic and anharmonic levels), as well as Pt-CO stretching harmonic frequencies (cm^{-1}). For adsorbed CO_2 surface species, only the highest CO stretching frequency has been evaluated at the anharmonic level. Note that CO frequencies are scaled due to the systematic predicted deviation obtained for gas phase CO with respect to measurements.

CO@Pt_1/CeO_{2-y}(hkl)	CeO_2(111)	CeO_{2-x}(111)	CeO_2(110)	CeO_2(211)	CeO_2(100)	CeO_2(210)
Adsorption site	top	top	top	top	bridge	bridge
Adsorption state	CO	CO	CO	CO	CO_2	CO_2
E_{ads} (eV)	-3.46	-0.94	-3.28	-3.10	-1.95	-2.20
M (μB)	0	2	0	2	2	-1.9
d(Pt-C) (Å)	1.81	1.90	1.80	1.81	2.02	2.05
d(Pt-O) (Å)	1.98	-	2.02	2.03	2.05	1.99;2.03
d(Pt-Ce) (Å)	-	3.01	-	-	-	-
d(C-O) (Å)	1.17	1.16	1.17	1.18	1.22;1.41	1.23;1.29
Scaled anharmonic CO stretching (cm^{-1})	2044	2041	2015	1982	1681	1747
Scaled harmonic CO stretching (cm^{-1})	2065	2065	2035	2002	1709	1754
Harmonic Pt-CO stretching (cm^{-1})	559	415	577	575	320	338

Hence our DFT models are validated from a spectroscopic point of view. However, CO adsorption on stepped surface such as $Pt_1/CeO_2(211)$ can provide a lower stretching frequency (1982 cm^{-1}) for linear top adsorption due to a strong chemisorption (large adsorption energy of -3.10 eV, and significantly elongated C-O distance of 1.18 Å). Such DFT value is closer to the range of measured bridge-bonded CO vibrations on the (111) facet of Pt nanoparticles (1875 cm^{-1}), raising the possibility that ceria support steps and defects might be contributing to the experimental measurements.

4. Conclusions

In summary, density functional theory calculations including strong electronic correlation semi-empirical correction model, spin polarization and van der Waals interactions have been reported to explore the stability of a single platinum atom on various ceria surfaces, including pristine, flat, stepped, reduced and neutralized systems. Adsorption thermodynamics as well as absolute stability descriptor have been predicted and compared via a systematic exploration of potential energy surfaces covering the stability of the metal over the whole ceria support.

Single platinum atoms exhibit the largest stability expressed in excess energy on the most stable ceria terminations, such as pristine and flat $CeO_2(111)$ and $CeO_2(110)$, for which the creation cost with respect to bulk ceria is minimal. Although the adsorption strength can reach -8 eV on stepped $CeO_2(210)$, the high metastability of such defective surfaces cannot be compensated by the adsorption of a single metallic atom. Thanks to the potential energy maps, diffusion kinetics have been evaluated and compared between the single platinum catalysts. The high stability of $Pt_1/CeO_2(111)$ and $Pt_1/CeO_2(110)$ is however linked to the high mobility of the single atom on these terminations, promoting the rapid formation of small clusters and their sintering. On the other hand, the stepped surfaces $CeO_2(211)$ and $CeO_2(210)$ inhibit the diffusion of platinum atoms, in favor of single atom catalysts, however their metastability is too high. Among the remaining terminations, the reduced $CeO_{2-x}(111)$ and stepped $CeO_2(100)$ offer a good compromise between intrinsic stability and moderately activated diffusion.

In line with this, our study of the formation of Pt dimer and trimer on the reduced $CeO_{2-x}(111)$ surface points out that the presence of oxygen vacancies may favor the growth of dimers, and prevent sintering.

To open the discussion regarding the Water-Gas-Shift reaction mechanism on ceria-based single platinum catalysts, a systematic study of adsorption and vibrations of the carbon monoxide has been addressed on the various single atom systems. While the large CO adsorption strength on Pt catalysts supported on pristine and flat $CeO_2(111)$ and $CeO_2(110)$ or stepped $CeO_2(211)$ explain their weak WGS activity, the reduced $CeO_{2-x}(111)$ appears as the best compromise for ensuring both sufficient stability of single atom catalysts and moderate adsorption of CO reactants. The computed vibrational analysis directly compared to available measurements provides important validation of our DFT models, while also bringing new spectroscopic features helpful to interpret infrared measurements. This work invites experimentalists to explore tailored, stepped and defective ceria terminations in the context of the rational design of more efficient single atom catalysts active for the Water-Gas-Shift reaction.

Acknowledgments

The authors acknowledge financial support from Agence National de la Recherche (ANR-19-CE05-0038 PRCI DYCAT project) and the Deutsche Forschungsgemeinschaft (DFG 431423888 DYCAT project). The authors thank the DYCAT partners at IRCELYON and KIT for fruitful

discussions. Access to national HPC resources of IDRIS and TGCC in Paris and CINES in Montpellier was provided by GENCI (projects 609 and AD010813359). The authors acknowledge the PSMN mesocenter in Lyon for CPU time and assistance (CPER/SYSPROD 2015-2022 project No. 2019-AURA-P5B and AXELERA Pôle de compétitivité).

Conflict of interest statement

The authors declare no conflict of interest.

Supplementary Material

Complementary DFT+U calculations concerning clean ceria surfaces (symmetric slab models) in Table S1, analysis of magnetic states for single Pt atom on ceria surfaces in Table S2, for CO adsorption on Pt_1/CeO_{2-y}(hkl) surfaces in Table S3, potential energy maps (Figures S1, S3) and optimized structures (Figures S2, S4) for dimer Pt_2 and trimer Pt_3 on the reduced ceria (111) surface. Bader charge analysis in Table S4.

Data Availability Statement

The data that support the findings of this study are available in the supplementary material of this article.

ORCID

Antoine Salichon https://orcid.org/0009-0007-5106-8258
Agustin Salcedo https://orcid.org/0000-0001-5525-8605
Carine Michel https://orcid.org/0000-0002-4501-7194
David Loffreda https://orcid.org/0000-0001-9912-7965

GRAPHICAL ABSTRACT

Antoine Salichon, Agustin Salcedo, Carine Michel and David Loffreda

Theoretical Study of Structure Sensitivity on Ceria-Supported Single Platinum Atoms and its Influence on Carbon Monoxide Adsorption

DFT+U calculations are performed to explore the adsorption properties of single platinum atom supported on various flat and stepped ceria surfaces, as well as those of carbon monoxide on these single atom catalysts in the context of the water-gas shift reaction. Potential energy surfaces are computed to predict the nucleation and growth properties of small platinum clusters on the basis of diffusion kinetics. CO adsorption and vibrations are also examined and compared with available measurements.

GRAPHICAL ABSTRACT FIGURE

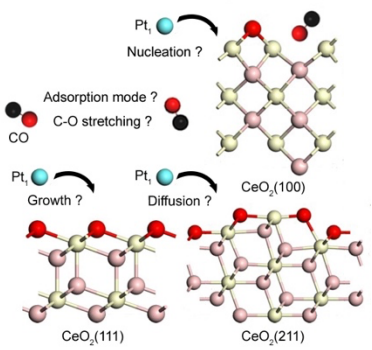

References and Notes

[1] H. Bjørkan, M. Rønning, H. J. Venvik, T. Johannessen, A. Holmen, *Catalysts* **2020**, *10*, 1132.
[2] M. Ziemba, C. Schilling, M. V. Ganduglia-Pirovano, C. Hess, *Acc. Chem. Res.* **2021**, *54*, 2884–2893.
[3] J. D. Holladay, Y. Wang, E. Jones, *Chem. Rev.* **2004**, *104*, 4767–4790.
[4] J. R. Ladebeck; J. P. Wagner, In Handbook of Fuel Cells – Fundamentals, Technology and Applications; W. Vielstich, A. Lamm, H.A. Gasteiger, Eds.; John Wiley & Sons: Chichester, **2003**; Vol. 3, Part 2, pp 190–201.
[5] V. Palma, C. Ruocco, M. Cortese, S. Renda, E. Meloni, G. Festa, M. Martino, *Metals* **2020**, *10,* 866.
[6] X. Wang, R. J. Gorte, J. P. Wagner, *Journal of Catalysis* **2002**, *212*, 225.
[7] P. Panagiotopoulou, D. I. Kondarides, *Catalysis Today* **2006**, *112*, 49–52.
[8] G. Ferré, M. Aouine, F. Bosselet, L. Burel, F. J. Cadete Santos Aires, C. Geantet, S. Ntais, F. Maurer, M. Casapu, J.-D. Grunwaldt, T. Epicier, S. Loridant, P. Vernoux, *Catal. Sci. Technol.* **2020**, *10*, 3904–3917.
[9] R. Jain, A. S. Poyraz, D. P. Gamliel, J. Valla, S. L. Suib, R. Maric, *Applied Catalysis A: General* **2015**, *507*, 1–13.
[10] D. B. Pal, R. Chand, S. N. Upadhyay, P. K. Mishra, *Renewable and Sustainable Energy Reviews* **2018**, *93*, 549–565.
[11] K. Yuan, Y. Guo, Q.-L. Lin, L. Huang, J.-T. Ren, H.-C. Liu, C.-H. Yan, Y.-W Zhang, *Journal of Catalysis* **2021**, *394*, 121–130.
[12] Y. M. Park, M. Son, M.-J. Park, J. W. Bae, *International Journal of Hydrogen Energy* **2020**, *45*, 26953–26966.
[13] Y. Li, M. Kottwitz, J. L. Vincent, M. J. Enright, Z. Liu, L. Zhang, J. Huang, S. D. Senanayake, W.-C. D. Yang, P. A. Crozier, R. G. Nuzzo, A. I. Frenkel, *Nature Communications* **2021**, *12*, 914.
[14] A. M. Gänzler, M. Casapu, P. Vernoux, S. Loridant, F. J. Cadete Santos Aires, T. Epicier, B. Betz, R. Hoyer, J.-D. Grunwaldt, *Angew.Chem.Int.Ed*. **2017**, *56*, 13078–13082.
[15] Y. Xin, N. Zhang, Y. Lv, J. Wang, Q. Li, Z. Zhang, *Journal of Rare Earths* **2020**, *38*, 850–862.
[16] A. Datye, Y. Wang, *Natl Sci Rev* **2018**, *5*, 630–632.
[17] L. Nie, D. Mei, H. Xiong, B. Peng, Z. Ren, X. I. Pereira-Hernandez, A. DeLaRiva, M. Wang, M. H. Engelhard, L. Kovarik, A. K. Datye, Y. Wang, *Science* **2017**, *358*, 1419–1423.
[18] T. Wu, X. Pan, Y. Zhang, Z. Miao, B. Zhang, J. Li, X. Yang, *J.Phys.Chem.Lett.* **2014**, *5*, 2479–2483.
[19] Z. Yang, T. K. Woo, M. Baudin, K. Hermansson, *J. Chem. Phys.* **2004***, 120*, 7741–7749.
[20] Y. Jiang, J. B. Adams, M. van Schilfgaarde, *J. Chem. Phys.* **2005**, *123*, 064701.
[21] S. Fabris, G. Vicario, G. Balducci, S. de Gironcoli, S. Baroni, *J. Phys. Chem. B* **2005**, *109*, 22860–22867.
[22] N. V. Skorodumova, M. Baudin, K. Hermansson, *Phys. Rev. B* **2004**, *69*, 075401.
[23] S.-H. Zhong, G. Lu, X.-Q. Gong, *Chinese Journal of Catalysis* **2017**, *38*, 1138–1147.
[24] D. Loffreda, F. Delbecq, *J. Chem. Phys.* **2012**, *136*, 044705.

[25] A. Bruix, Y. Lykhach, I. Matolínová, A. Neitzel, T. Skála, N. Tsud, M. Vorokhta, V. Stetsovych, K. Ševčíková, J. Mysliveček, R., Fiala, M. Václavů, K. C. Prince, S. Bruyère, V. Potin, F. Illas, V. Matolín, J. Libuda, K.M. Neyman, *Angew. Chem. Int. Ed.* **2014**, *53*, 10525–10530.
[26] F. Maurer, J. Jelic, J. Wang, A. Gänzler, P. Dolcet, C. Wöll, Y. Wang, F. Studt, M. Casapu, J.-D. Grunwaldt, *Nature Catalysis* **2020**, *3*, 824–833.
[27] A. Bruix, K. M. Neyman, F. Illas, *The Journal of Physical Chemistry C* **2010**, *114*, 14202–14207.
[28] F. Dvorak, M. F., Camellone, A. Tovt, N.-D. Tran, F. R. Negreiros, M. Vorokhta, T. Skala, I. Matolinova, J. Myslivecek, V. Matolin, S. Fabris, *Nature Communications* **2016**, *7*, 10801.
[29] A. Tovt, L. Bagolini, F. Dvorak, N.-D. Tran, M. Vorokhta, K. Beranova, V. Johanek, M. F. Camellone, T. Skala, I. Matolinova, J. Myslivecek, S. Fabris, V. Matolin, *Journal of Materials Chemistry A* **2019**, *7*, 13019–13028.
[30] X. Wang, J. A. van Bokhoven, D. Palagin, *Phys. Chem. Chem. Phys.* **2020**, *22*, 28–38.
[31] A. Bruix, A. Migani, G. N. Vayssilov, K. M. Neyman, J. Libudade, F. Illas, *Phys. Chem. Chem. Phys.* **2011**, *13*, 11384–11392.
[32] A. Bruix, J. A. Rodriguez, P. J. Ramírez, S. D. Senanayake, J. Evans, J. B. Park, D. Stacchiola, P. Liu, J. Hrbek, F. Illas, *Journal of the American Chemical Society* **2012**, *134*, 8968–8974.
[33] D. Kunwar, S. Zhou, A. DeLaRiva, E. J. Peterson, H. Xiong, X. I. Pereira-Hernández, S. C. Purdy, R. ter Veen, H. H. Brongersma, J. T. Miller, H. Hashiguchi, L. Kovarik, S. Lin, H. Guo, Y. Wang, A. K. Datye, *ACS Catal.* **2019**, *9*, 3978–3990.
[34] S. Yoon, H. Ha, J. Kim, E. Nam, M. Yoo, B. Jeong, H. Y. Kim, K. An, *Journal of Materials Chemistry A* **2021**, *9*, 26381–26390.
[35] P. Castro-Latorre, K.M. Neyman, A. Bruix, *The Journal of Physical Chemistry C* **2023**, *127*, 17700–17710.
[36] A. Bruix; F. Nazari; K. M. Neyman; F. Illas, *J. Chem. Phys.* **2011**, *135*, 244708.
[37] D. Ma, T. Li, Q. Wang, G. Yang, C. He, B. He, Z. Lu, Z. Yang, *Applied Surface Science* **2017**, *394*, 47–57.
[38] Y.-Y. Qin, Y.-Q. Su, *ChemCatChem* **2021**,*13*, 3857–3863.
[39] R. T. Kinch, C. R. Cabrera, Y. Ishikawa, *J. Phys. Chem. C* **2009**, *113*, 9239–9250.
[40] S. Aranifard, S. C. Ammal, A. Heyden, *J. Phys. Chem. C* **2012**, *116*, 9029–9042.
[41] S. Aranifard, S. C. Ammal, A. Heyden, *Journal of Catalysis* **2014**, *309*, 314–324.
[42] J. Vecchietti, A. Bonivardi, W. Xu, D. Stacchiola, J. J. Delgado, M. Calatayud, S. E. Collins, *ACS Catal.* **2014**, *4*, 2088–2096.
[43] D.-Y. Wei, M.-F. Yue, S.-N. Qin, S. Zhang, Y.-F. Wu, G.-Y. Xu, H. Zhang, Z.-Q. Tian, J.-F. Li, *J. Am. Chem. Soc.* **2021**, *143*, 15635–15643.
[44] Y. Tang, Y.-G. Wang, J. Li, *J. Phys. Chem. C* **2017**, *121*, 11281–11289.
[45] Y. Lu, S. Zhou, C.-T. Kuo, D. Kunwar, C. Thompson, A. S. Hoffman, A. Boubnov, S. Lin, A. K. Datye, H. Guo, A. M. Karim, *ACS Catal.* **2021**, *11*, 8701–8715.
[46] I. Z. Koleva, H. A. Aleksandrov, G. N. Vayssilov, *ACS Catal.* **2023**, *13*, 5358–5374.
[47] G. Kresse, J. Hafner, *Physical Review B* **1993**, *47*, 558.
[48] G. Kresse, J. Hafner, *Physical Review B* **1994**, 49, 14251.
[49] G. Kresse, J. Furthmüller, *Computational Materials Science* **1996**, *6*, 15.
[50] G. Kresse, J. Furthmüller, *Physical Review B* **1996**, *54*, 11169.
[51] J. P. Perdew, K. Burke, M. Ernzerhof, *Physical Review Letters* **1996**, *77*, 3865.

[52] S. Grimme, J. Antony, S. Ehrlich, H. Krieg, H., *The Journal of Chemical Physics* **2010**, *132*, 154104.
[53] S. Grimme, S. Ehrlich, L. Goerigk, *Journal of Computational Chemistry* **2011**, *32*, 1456.
[54] S. L. Dudarev, G. A. Botton, S. Y. Savrasov, C.J. Humphreys, A. P. Sutton, *Physical Review B* **1998**, *57*, 1505–1509.
[55] N. V. Skorodumova, S. I. Simak, B. I. Lundqvist, I. A. Abrikosov, B. Johansson, *Physical Review Letters* **2002**, *89*, 166601.
[56] M. Nolan, S. C. Parker, G.W. Watson, *Surface Science* **2005**, *595*, 223.
[57] C. Loschen, J. Carrasco, K. M. Neyman, F. Illas, *Physical Review B - Condensed Matter and Materials Physics* **2007**, *75*, 1.
[58] M. V. Ganduglia-Pirovano, A. Hofmann, J. Sauer, *Surface Science Reports* **2007**, *62*, 219–270.
[59] M. V. Ganduglia-Pirovano, J. L. F. D. Silva, J. Sauer, *Physical Review Letters* **2009**, *102*, 02610.
[60] S. Fabris, G. Vicario, G. Balducci, S. de Gironcoli, S. Baroni, *The Journal of Physical Chemistry B* **2005**, *109*, 22860–22867.
[61] M. Cococcioni, S. de Gironcoli, *Physical Review B* **2005**, *71*, 035105.
[62] G. Kresse, D. Joubert, *Physical Review B* **1999**, *59*, 1758–1775.
[63] Z.Yang, T. K. Woo, M. Baudin, K. Hermansson, *J. Chem. Phys.* **2004**, *120*, 7741–7749.
[64] I. Z. Koleva, H. A. Aleksandrov, G. N. Vayssilov, *Catalysis Today* **2020**, *357*, 442–452.
[65] M. Happel, J. Mysliveček, V. Johánek, F. Dvořák, O. Stetsovych, Y. Lykhach, V. Matolín, J. Libuda, *Journal of Catalysis* **2012**, *289*, 118–126.
[66] D. W. Daniel, *J. Phys. Chem.* **1988**, *92*, 3891–3899.
[67] O. Brummel, F. Waidhas, F. Faisal, R. Fiala, M.Vorokhta, I. Khalakhan, M. Dubau, A. Figueroba, G. Kovács, H. A. Aleksandrov, G. N. Vayssilov, S. M. Kozlov, K.M. Neyman, V. Matolín, J. Libuda, *J. Phys. Chem. C* **2016**, *120*, 19723–19736.